SHIELDING MECHANISMS IN MIXED MODE INTERFACIAL FRACTURE

J. G. SWADENER and K. M. LIECHTI
Engineering Mechanics Research Laboratory
Department of Aerospace Engineering and Engineering Mechanics
The University of Texas at Austin, Austin, Texas 78712-1085 USA

ABSTRACT

An increase in apparent fracture toughness with increasing mode II component of loading has been observed by several investigators in interfacial fracture. In this study, cracks were grown in a steady state manner along the glass/epoxy interface in sandwich specimens in order to determine the mechanisms responsible for the shielding effect. Finite element analysis using a continuum plasticity model and a cohesive zone model for debonding shows that plastic dissipation in the epoxy can account for the shielding seen in these experiments which cover a wide range of mode-mix. Measurements of crack opening displacements close to the crack tip give results consistent with the analytical predictions.

KEYWORDS

Interfacial fracture, fracture toughness, mixed mode, shielding, plastic dissipation

INTRODUCTION

This study is part of an ongoing examination of the mechanisms responsible for interfacial fracture toughness. The motivation comes from the common occurrence of interfacial fracture in composites, microelectronics and pressure sensitive adhesives and from even more common cohesive failures near an interface which possess many of the same features. A number of studies, e.g. Cao and Evans (1989) and Wang and Suo (1990), have determined that interfacial toughness is a function of mode-mix. Liechti and Chai (1991,1992) have considered nearly a full range of mode-mix in bimaterial specimens, but the mechanism responsible for toughening remains unclear. Proposed shielding mechanisms include plasticity, viscoelasticity, asperity locking, the effect of constraining layers, and electrostatic surface charges. Each of these will be addressed, but the emphasis will be on plasticity which appears to dominate in the cases studied herein. Sandwich specimens are used, because the stiff layers cause an increase in stress concentration for small applied displacements. This allows for better observation of the normal crack opening displacements (NCOD) near the crack tip.

EXPERIMENTAL PROCEDURE

The sandwich specimens tested in this study were composed of glass and aluminum with a relatively thin epoxy bond line as shown in fig. 1. The epoxy height, h_2, ranges from 0.13 to

0.40 mm. The epoxy is composed of a modified bisphenol A resin which contains dibutyl phthalate as a plasticizer and a polyamido amine hardener (CIEBA-GEIGY products Araldite GY502 and HY95). The specimens were pre-cracked a minimum of 8 mm along the glass/epoxy interface. For this ratio of a/h_2, fracture parameters have been shown by Knauss (1966) and Rice (1968) to be independent of crack length. Displacements (u, v) were applied to the specimen via steel grips in both the bond-tangential (x-) direction and the bond-normal (y-) direction in the same manner as described by Liechti and Chai (1991). Sufficient displacements were applied to initiate and maintain crack propagation. The crack was grown for a few millimeters so that steady state conditions were achieved. The length of crack propagation was also sufficient so that the previous plastic deformations did not affect the current test point. Crack growth was maintained along the interface. After acquiring data, the displacements were reduced and the crack arrested. Thus it was possible to perform several experiments with different values of mode-mix on the same specimen.

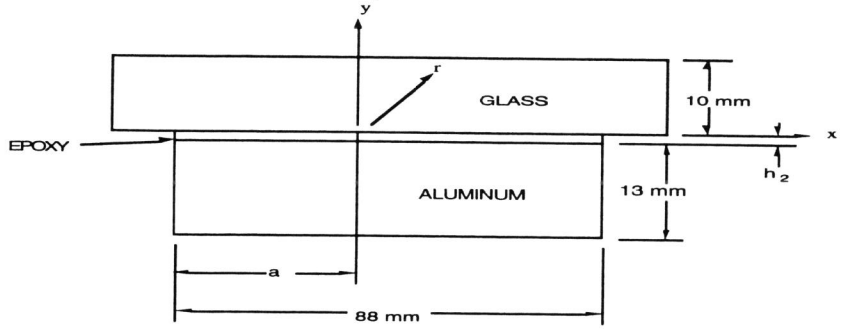

Specimen thickness 5.6 mm

Fig. 1 Specimen Geometry

NCOD were measured using crack opening interferometry (Liechti, 1993). The interference fringes produced by crack opening interferometry were viewed through a microscope and recorded by using a 500 line video cassette recorder. Depending on the magnification used, the spatial resolution ranged from 1.1 to 4.8 μm. A digital image analyzer made possible the determination of NCOD to 1/100 of a fringe order, which gave a resolution of 3 nm. However, uneven reflections from the aluminum adherend caused greater scatter in the NCOD measurements, essentially yielding an accuracy of 5 nm.

ANALYSIS

From the invariance of the J-integral under small scale yielding conditions (Rice, 1968), the energy release rate is found in terms of the displacement of the grips as:

$$G = \frac{v^2}{2}\left(\frac{h_1}{\hat{E}_1} + \frac{h_2}{\hat{E}_2} + \frac{h_3}{\hat{E}_3}\right) + \frac{u^2}{2}\left(\frac{h_1}{\mu_1} + \frac{h_2}{\mu_2} + \frac{h_3}{\mu_3}\right), \qquad (1)$$

where $\hat{E}_i = 2\mu_i/(1-\nu_i)$ for plane stress and $\hat{E}_i = 2\mu_i(1-\nu_i)/(1-2\nu_i)$ for plane strain, μ_i is the shear modulus of component i and ν_i is its Poisson's ratio.

The mode-mix is expressed in terms of the angle ψ defined by: $\psi = \tan^{-1}\left(\frac{K_2}{K_1}\right) + \varepsilon \ln\left(\frac{\hat{l}}{h_2}\right)$,

where ε is the bimaterial constant, $\hat{l}$ is a material length parameter which we choose arbitrarily as 100 μm. The value of ψ is extracted from finite element analyses using the method of Yau and Wang (1984).

The component of the energy release rate due to plastic dissipation, G_p, is found from finite element analysis of a 48 mm length of the specimen which contains a crack growing at a prescribed constant speed. G_p is calculated as $W_p/b\cdot\Delta a$, where W_p is the plastic dissipation energy, b is the model width and Δa is the increment of crack growth. The finite element code ABAQUS under academic license from Hibbitt, Karlsson and Sorensen, Inc. is used. The analysis is quasi-static under the condition of plane strain.

Glass and aluminum components are modeled as elastic elements since they do not exceed the elastic limit in the cases studied. Material properties are shown in table 1. A user material subroutine is used to capture the hydrostatic stress and strain rate dependencies of the epoxy. The hydrostatic stress dependence is an extended version of the Drucker-Prager model based on the theory given in the ABAQUS Users' Manual (1992), i.e. the flow potential is: $g = t - p\tan\phi$, where

$$t = \left(\frac{1}{2}\right)q\left[1 + R - (1 - R)\left(\frac{r}{q}\right)^3\right]$$

is an equivalent stress measure, $p = -\mathrm{tr}(\underline{\sigma})/3$, $q = \frac{3}{2}(\underline{s}:\underline{s})^{1/2}$, $r^3 = \frac{9}{2}\underline{s}:(\underline{s}:\underline{s})$, $\underline{s}$ is the deviatoric stress tensor, R (= 1.04) is the ratio of yield strength in compression to that in tension, and ϕ is the angle to the t-axis in the p-t plane specifying the direction the yield surface grows. We use fully associated flow with $\phi = \beta = \tan^{-1} 3(R-1)$, where β is the angle of the slip plane. The strain rate dependence is given in rate form as:

$$\dot{\underline{\varepsilon}}^p = \left[\frac{D}{R(1+\frac{1}{3}\tan\beta)}\right]\left(\frac{\sigma_t}{\sigma_0} - 1\right)^n \frac{\frac{\partial f}{\partial \underline{\sigma}}}{\left(\frac{\partial f}{\partial \underline{\sigma}}:\frac{\partial f}{\partial \underline{\sigma}}\right)^{1/2}},$$

where $\dot{\underline{\varepsilon}}^p$ is the plastic strain rate, σ_t is the current equivalent flow stress in tension, σ_0 is the quasi-static flow stress, and $f = t - \tan\beta$. The values for the material parameters n (= 8.98) and D (= 0.29 s^{-1}) were found by Liang and Liechti (1996) from shear tests. Hardening is isotropic and follows their plane-strain compression experimental results. The analysis uses the Jaumann stress rate which has been shown by several authors not to be accurate for large strains (for a review see Naghdi, 1990), but should give correct results for the cases we study where the strains do not exceed 30% (see Schieck and Stumpf, 1995).

Table 1 Material Properties

Material	Elastic Modulus	Poisson's Ratio
Glass	69 GPa	0.2
Epoxy	2.03 GPa	0.36
Aluminum	70 GPa	0.3

The plasticity equations are integrated using a modified theta scheme developed by Kanchi et al (1978):

$$\left\{ [\underline{D}^{el}]^{-1} + \theta \Delta t \left. \frac{\partial \dot{\underline{\varepsilon}}^{p}}{\partial \sigma} \right|_{t} \right\} : \Delta \underline{\sigma} = \Delta \underline{\varepsilon} - \Delta t \, \dot{\underline{\varepsilon}}^{p}|_{t} \, ,$$

where θ is chosen to be 0.5, $\underline{D}^{el}$ is the elastic compliance matrix, Δt is the time increment, $\Delta \underline{\varepsilon}$ is the increment of strain, and $\Delta \underline{\sigma}$ is the resulting increment of stress. All quantities are evaluated explicitly at time t. This scheme converges for reasonable values of Δt for our problem.

The debonding process is not well understood and occurs on the nanoscale which is too small to capture completely with a continuum model. Therefore a cohesive zone model is used for debonding . A molecular modeling method might be preferable, but the interaction of glass and epoxy molecules is not yet known. With crack propagation prescribed as a function of time, tractions across the interface are released linearly with time. This results in a nearly linear traction displacement relation on the crack surfaces. We do not propose that this is the actual interaction of the surfaces, but merely that it gives results which are adequate for the evaluation of the shielding mechanisms. Tvergaard and Hutchinson (1994) have shown that fracture toughness results are not strongly dependent on the shape of the traction-separation relationship. To model steady state crack growth, we set the time to release the tractions completely to be a constant. This gives a cohesive zone of constant length.

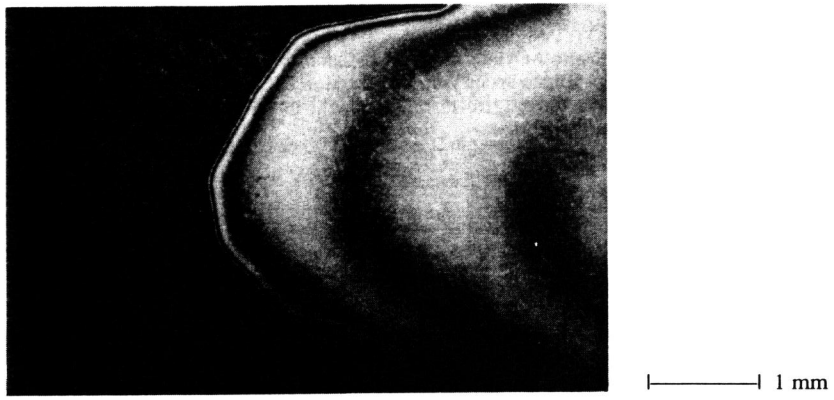

Fig. 2 Fringe patterns obtained by crack opening interferometry

RESULTS AND DISCUSSION

An example of the fringe patterns observed is shown in fig. 2. The crack front is the dark edge ahead of the first bright fringe and is seen to be curved. This was the case for most experiments, but this shape would propagate in a self-similar manner. We find that in the K-dominant zone (< 100 μm), plane strain and 3D finite element analyses give essentially identical results away from the free surfaces provided the radius of the crack front is 400 μm or greater. Therefore we use plane strain analyses and data taken from the center of the crack front. NCOD results for two growing cracks are compared to plane strain finite element predictions in fig. 3. The predictions are for two different lengths of the cohesive zone: α = 0.25 and 0.5 μm. A finite element mesh using 4 node bilinear quadrilateral elements with a minimum size of 31 nm was used. The experimental results agree with the predictions to within 1.1 μm of the crack tip which is the

spatial resolution used. These results are not adequate to determine the exact value for α, but they do show that its value should be less than 1 μm. The plastic zone is found to extend less than 0.5 μm behind the crack tip, thus it also cannot be seen in the results.

The fracture toughness varies somewhat from specimen to specimen, but was the same for these two results which were for different bond thicknesses. Tvergaard and Hutchinson (1994) have shown that shielding will occur when the plastic zone size is greater than 1/5 the bond thickness. However, the largest plastic zone size found in this study was 13 μm which was only 1/20 of the bond thickness.

Liang and Liechti (1995) reported unusual reduced NCOD measurements near the crack tip in bimaterial specimens and postulated the existence of electrostatic charges on the crack surfaces. Similar NCOD behavior was observed in our preliminary experiments with sandwich specimens, but when higher magnification and sharper focus were used, the NCOD results were generally similar to those shown in fig. 3. Additionally, the air in the vicinity of the crack faces was ionized with a Po-210 α-radiation source. The ionized air was drawn through the crack with suction. This did not cause any observable changes in the NCOD. Therefore, if electrostatic charges of significant magnitude exist, they must be confined to within approximately 1 μm of the crack tip.

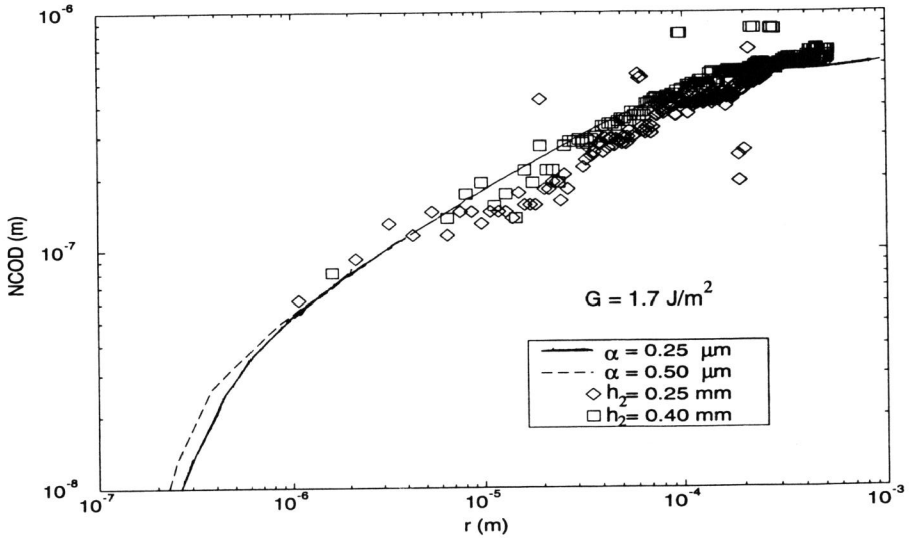

Fig. 3 NCOD results for two cracks with $\psi = 40^{\circ}$

Fracture toughness, normalized by its value for bond-normal loading (G_0), is plotted versus crack speed in fig. 4. For predominantly mode I loading, little or no affect of crack speed is observed. This is expected, because plasticity has a small affect for these cases. For loading with greater mode II components, the plasticity effect is greater and some decrease of fracture toughness with increasing crack speed can be seen, although there is considerable scatter, particularly for $\psi = -50^{\circ}$.

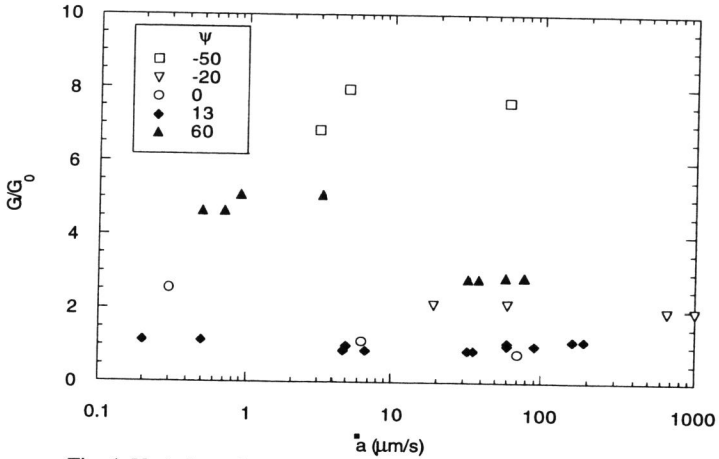

Fig. 4 Variation of normalized fracture toughness with crack speed

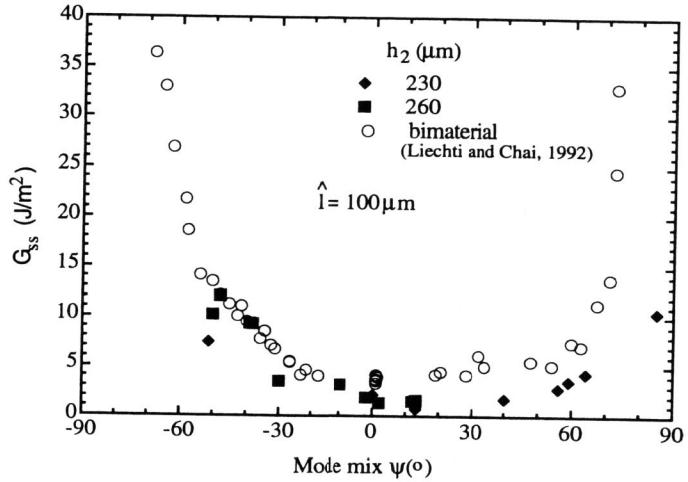

Fig. 5 Fracture toughness values for sandwich and bimaterial specimens

Fracture toughness values versus mode-mix are shown in fig. 5 for sandwich specimens with similar bond normal fracture toughness. Comparison with the results for bimaterial specimens from Liechti and Chai (1992) shows similar asymmetric shielding with mode-mix. The sandwich specimen curve appears to be shifted +15° compared to the bimaterial results. Setting $\hat{l}$ = 10 mm would bring the two curves into alignment, but this value seems too large for a material length scale. Both the volume of the active plastic zone and the strain (for a fixed r) increase with the Mode II component of loading. But the increase is not as dramatic as in the fracture toughness where these effects are combined.

Figure 6 shows the shielding affect of plasticity for selected points. When α is set equal to 0.5 μm, plastic dissipation accounts for the variation of fracture toughness with mode-mix. The variation of G_p with ψ also mirrors the asymmetric aspects of the total value of G within the resolution of the experiments. If α is decreased to 0.25 μm, the plastic dissipation is too great at the largest magnitudes of mode-mix. The resultant (G - G_p) is in the range of 1 to 2 J/m^2. This is too large to be accounted for by surface energy alone which was found by Schnapp (1996) to be approximately 0.1 J/m^2.

Also, there must be an additional dissipative mechanism to explain the steady state crack growth observed in the experiments. The strain rate dependence in the continuum model gives decreased plastic dissipation at higher crack speeds, and therefore cannot account for stable crack propagation. Asperity shielding and viscoelastic dissipation were shown by Liechti and Chai (1992) to be negligible. Friction, electrostatics and inelastic material deformation on the nanoscale within the cohesive zone region are possible additional mechanisms. Fortunately, however, the energy dissipated by the additional mechanism(s) does not appear to vary with mode-mix. Therefore, two simple experiments (one predominantly mode I and the other with a significant mode II component) could establish the length to use for the cohesive zone. Then finite element analysis using continuum material models and a simple cohesive zone model, could be used to determine the fracture toughness at any desired mode-mix.

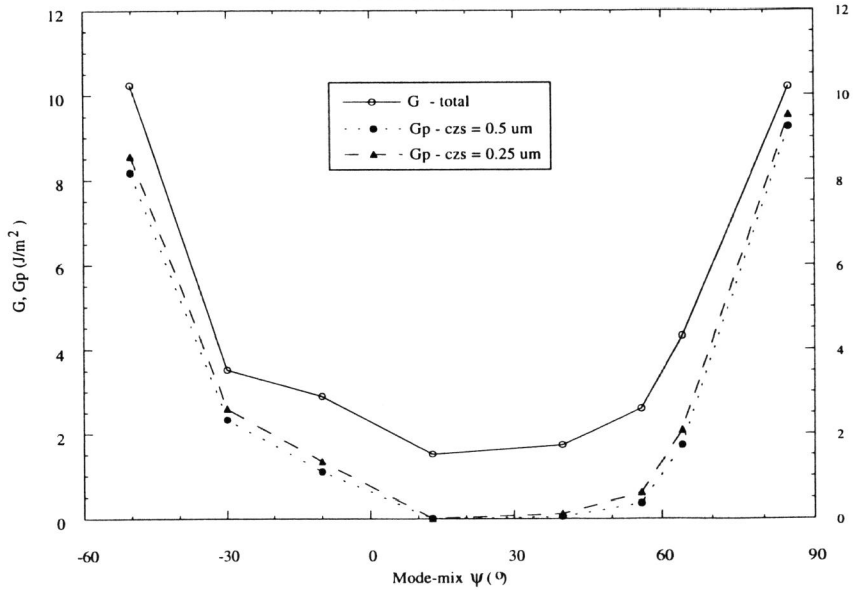

Fig. 6 Plastic dissipation component of fracture toughness

CONCLUSIONS

Interfacial cracks in sandwich specimens have been observed during stable self-similar growth with a spatial resolution of as low as 1.1 μm. The results indicate that the length of the cohesive zone is less than 1 μm.

Asymmetric shielding has been observed in these specimens, similar to the results of Liechti and Chai (1992) with bimaterial specimens. The shielding can be accounted for by plastic dissipation when hydrostatic stress and strain rate dependencies are included. The choice of the cohesive zone length has not yet been verified experimentally and will be the subject of further study. A value of $\alpha = 0.5$ μm gave the best agreement with experimental data and fits within the range of possible lengths. Continuum plasticity does not account for all of the energy dissipated during fracture, but the remainder does not appear to vary with mode-mix. Therefore it is possible to predict the variation of fracture toughness for the complete range of mode-mix from two simple experiments and using continuum models for the materials in interfacial fracture under small scale yielding conditions.

ACKNOWLEDGMENT

The authors would like to acknowledge the financial support for this work provided by the National Science Foundation.

REFERENCES

Cao, H. C. and A. G. Evans (1989). An experimental study of the fracture resistance of bimaterial interfaces. *Mechanics of Materials*, **7**, 295 -304

Hibbitt, Karlsson and Sorensen Inc. (1992). ABAQUS User's Manual, Pawtuket, RI

Kanchi, M. B., O. C. Zienkiewicz and D. R. J. Owen (1978). The viscoplastic approach to problems in plasticity and creep involving geometric non-linear effects. *Int. J. Num. Meth. Engrg.*, **12**, 169-181

Knauss, W. G. (1966). Stresses in an Infinite Strip Containing a Semi-Infinite Crack. *J.. Appl. Mech.*, **33**, 356-362.

Liang, Y.-M. and K. M. Liechti (1995). Toughening mechanisms in mixed-mode interfacial fracture. *Int. J. Solids and Structures*, **32**, 957-978

Liang, Y.-M. and K. M. Liechti (1996). On the large deformation and localization behavior of an epoxy resin under multiaxial stress states. *Int. J. Solids and Structures*, **32**, 1479-1500

Liechti, K. M. (1993). Chapter 4 in Experimental Techniques in Fracture (ed. J. S. Epstein), VCH Publishers, New York

Liechti, K. M. and Y.-S. Chai (1991). Biaxial loading experiments for determining interfacial fracture toughness. *J. Appl. Mech.*, **58**, 680-687

Liechti, K. M. and Y.-S. Chai (1992). Asymmetric shielding in interfacial fracture under in-plane shear. *J. Appl. Mech.*, **59**, 295-304

Naghdi, P. M. (1990). A critical review of the state of finite plasticity. *J. Appl. Math. Phys.* (ZAMP), **41**, 315-394.

Rice, J. R. (1968). A path independent integral and the approximation analysis of strain concentrations by notches and cracks, *J.. Appl. Mech.*, **35**, 379-386.

Schieck, B. and H. Stumpf (1995). The appropriate corrotational rate, exact formula for the plastic spin and constitutive model for finite elastoplasticity, *Int. J. Solids and Structures*, **32**, 3643-3667.

Schnapp, S. T. (1996). *Thesis*, U. Texas at Austin.

Tvergaard, V. and J. W. Hutchinson (1994). Toughness of an interface along a thin ductile layer joining elastic solids. *Phil. Mag. A*, **70**, 641-656.

Wang, J.-S. and Z. Suo (1990). Experimental determination of interfacial toughness using Brazil-nut sandwiches. *Acta Metall. Mater.*, **38**, 1279-1290.

Yau, Y. F. and S. S. Wang (1984).An analysis of interface cracks between dissimilar isotropic materials using conservation integrals in elasticity. *Eng. Fracture Mech.*, **20**, 423-432.